PCCP

PAPER

View Article Online
View Journal | View Issue

Cite this: *Phys. Chem. Chem. Phys.*, 2026, **28**, 4054

Influence of solid helium on the luminescence of nitrogen–neon nanoclusters

Oleksandr Korostyshevskyi,* Cameron K. Wetzel, David M. Lee and Vladimir V. Khmelenko

Received 11th November 2025,
Accepted 26th January 2026

DOI: 10.1039/d5cp04357c

rsc.li/pccp

We studied the luminescence of neon nanoclusters doped with nitrogen atoms. Neon nanoclusters were collected inside bulk superfluid helium at temperatures below 1.5 K. We found that the spectra of the nitrogen atom α-group had a specific shape with an enhanced narrow line at λ = 519.9 nm. The measured spectroscopic characteristics of this line, such as the position, narrow linewidth, relatively large intensity, and long lifetime, allow assignment of this line to nitrogen atoms on the surfaces of neon nanoclusters, surrounded by layers of solid helium. This is the first observation of the influence of solid helium on the spectral characteristics of atoms inside the bulk superfluid helium.

1 Introduction

Matrix isolation of impurities in condensed helium is a fascinating area of research.[1–6] Historically, the first studies of impurity species immersed in bulk liquid helium were performed by α-particle bombardment of colloidal particles suspended in liquid helium, and the emission spectra of N_2 and O_2 molecules immersed in liquid helium were observed.[7] A systematic study of atoms stabilized in superfluid helium (HeII) was carried out using the method of injection of the products of gaseous discharge into HeII.[8,9] Optical spectroscopy, electron spin resonance (ESR), ultrasonic, and x-ray studies were used for characterization of the impurity structures formed in liquid helium.[5] Initially, it was suggested that impurities form an impurity-helium solid phase, which consists of solid helium surrounding the impurities.[10–12] However, X-ray and ultrasound investigations of the samples formed by impurities in HeII provided evidence that the impurities formed nanoclusters with sizes of 5–6 nm, building a porous aerogel-like structure inside liquid helium.[13–19] Most of the stabilized chemically active atoms resided on the surfaces of nanoclusters.[20–22] It was suggested that one or two layers of solid helium were formed on the surfaces of the impurity nanoclusters, providing the stability of atoms in the porous structures. Later spectroscopic studies of alkali and alkali-earth atoms and ions embedded into HeII and solid helium were performed.[1–3,6] The observed absorption and emission spectra of atoms embedded into condensed helium were explained in the "bubble" model.[1,6]

Interest in the investigation of embedded into HeII atoms, molecules, and clusters was increased after the implementation of impurity doping into helium nanodroplets.[2,4,23–27] This method allows studies of the properties of liquid helium as well as optical and magnetic characteristics of atoms and molecules captured in liquid He nanodroplets. Helium nanodroplets have been used for investigations of atomic and molecular aggregation, since they provide a high degree of control of the aggregation process, efficient cooling to 0.37 K, and enable measurements with low matrix effect, compared to other noble gas environments.[2,28,29]

In the studies of atoms and molecules in liquid helium, a question arises about the structure of helium surrounding the impurities. Depending on the interaction between the impurity and the surrounding liquid helium, the solvation structure can be divided into two different cases. The "bubble" structure is observed for impurities with mostly repulsive interactions with helium, however, the "snowball" structure forms around impurities exhibiting strongly bound potentials with helium.

In this article, we are focusing on the impurities that have attractive potential with the surrounding helium. The formation of a solvated layer around an impurity exhibiting strongly bound potential toward helium has been studied theoretically using different approaches.[30–35] The pronounced shell structure of He atoms around a single Xe atom was predicted.[30] Later, by using a density functional theory, it was shown that in bulk liquid helium, all rare gas atoms are surrounded by strongly bound helium shells in which helium densities are equal to or exceed the solid helium density.[32] Furthermore, the possibility of a quantum gel, formed from impurities surrounded by solid helium, was discussed in the literature.[33] Fluorine and neon atoms were suggested as good candidates for impurity-based quantum gels.[34,35] A problem of the collapse of He shells

Institute for Quantum Science and Engineering, Department of Physics and Astronomy, Texas A&M University, College Station, TX, 77843, USA.
E-mail: korostyshevskyi@tamu.edu

surrounding the impurity atoms and the formation of clusters of impurities in liquid helium was also discussed theoretically. The formation of Ne_2 van der Waals complexes inside superfluid helium was considered recently, and conclusions were made about the possibility of the formation of "quantum gel"/"quantum foam" where a layer of solid helium separates neon atoms.[36]

The dynamics of argon atoms clustering in superfluid ^{4}He nanodroplets were investigated in real time using the density functional approach applied to liquid helium. Depending on the initial kinematic conditions, two different argon structures can be formed: either a compact Ar cluster, or a loosely bound metastable cluster with dense helium cage inside.[37] In summary, there are theoretical predictions for the existence of structures formed by helium "snowballs" surrounding the impurity species.

Recently, experimental evidences for the existence of structures formed by the solvation helium layers surrounding impurity atoms in helium nanodroplets were found. The first example was the observation of a foam structure by doping helium nanodroplets with Mg atoms.[38–41] In the foam structure, the Mg atoms are separated by layers of He atoms. The distance between the Mg atoms in the structure was found to be about 1 nm. The electronic and optical properties of the Mg atoms in the foam are similar to those of a single atom, as demonstrated by resonance two-photon ionization in the vicinity of the atomic transition. The metastable network of Mg atoms undergoes spontaneous collapse upon illumination by laser radiation.[38,39] As a result, Mg_n clusters are formed in the relaxation process. In contrast, recent studies of the infrared spectra of magnesium-doped superfluid helium nanodroplets, with different sizes and numbers of dopants, were consistent with the formation of compact magnesium clusters.[42]

The second experimental evidence for the foam structure was obtained from electron diffraction studies of Xe-doped helium nanodroplets with sizes in the range of 10^5–10^6 helium atoms and xenon structures containing up to one hundred atoms.[43,44] For reliable fitting of some recorded diffraction patterns, in addition to the Xe–Xe and Xe–He distances, longer distances between Xe atoms, such as Xe–He–Xe and Xe–He–He–Xe, should be included. This fact supports the observation of the Xe foam structure.

The experimental approach for forming macroscopic quantities of quantum gel (foam structure) can be similar to that used in the work on the injection of impurity helium gas mixtures into bulk superfluid helium.[8,9] Only the concentrations of impurities in the impurity-helium gas mixtures should be reduced substantially in comparison with the previous experiments. Reducing the concentration of the impurities prevents the formation of nanoclusters and can lead to the realization of the conditions for the injection of individual atoms or molecules into bulk superfluid helium. All previous experiments were performed with impurity-helium gas mixtures containing 1% or more impurity. As a result, only collections of impurity nanoclusters were observed in bulk HeII.[5,13] Even in these conditions, the impurity nanoclusters were covered by at least one layer of solid helium. Further dilution of impurities by helium gas in the condensed gas mixture should reduce the size of impurity clusters injected into HeII and increase the quantity of solid helium in HeII.

To date, there have been no direct observations of the influence of solid helium on the characteristics of impurities collected in HeII. Searching for evidence of a solid helium layer surrounding impurities or clusters of impurities in superfluid helium is a challenging task. Recently, we studied the luminescence of nitrogen–neon nanoclusters immersed in bulk HeII. We studied the α-group spectra of N atoms corresponding to the $^2D \rightarrow {}^4S$ transitions. The spin and parity forbidden $^2D \rightarrow {}^4S$ transitions of N atoms in the solid matrices gave rise to a group of lines with wavelength in the range 519–523 nm. These lines correspond to the emission of nitrogen atoms in different trapping sites of the solid matrices.[45–48] The N_2/Ne ratios in nitrogen–neon nanoclusters were 10% and 20%. The observed α-group spectra of N atoms were fitted by seven components. It was found that the narrow component at λ = 519.9 nm prevails at the late stages of luminescence decay.[49] Tentatively, this spectral component was assigned to nitrogen atoms stabilized on the surfaces of neon nanoclusters surrounded by a layer of solid helium. The characteristic of these nitrogen atoms might be influenced by interaction with the solid helium layer surrounding the neon nanoclusters.

In the present work, we performed a comprehensive study of the luminescence of neon nanoclusters immersed in bulk HeII. A small amount of nitrogen atoms were added to the Ne nanoclusters as a probe. The α-group spectra of N atoms stabilized in Ne nanoclusters immersed in bulk HeII were studied for nanoclusters with different N_2/Ne ratios ranging from 0.016% to 5%. We found that the shape of α-group spectra was similar for all studied nitrogen–neon nanoclusters with a small content of N atoms. The component at λ = 519.9 nm was the largest in all the studied α-group spectra. The lifetime of this component was $\approx$280 s, the position of this component was close to that of the N atom in the gas phase, which has a much longer decay time ($\approx$44 hours). The above facts allow us to suggest that for the first time we observed N atoms in bulk HeII, whose characteristics are influenced by solid helium.

2 Experimental setup

The optical spectroscopy studies presented in this work were conducted in a glass helium Dewar.[50–52] The experimental setup was described in detail elsewhere.[52] The helium Dewar was surrounded by another Dewar, filled with liquid nitrogen, as shown in Fig. 1. The collections of nitrogen–neon nanoclusters were accumulated in a small 15 mL quartz beaker (9 in Fig. 1) located within the helium Dewar. The level of liquid helium in the Dewar was kept below the quartz beaker for the duration of the experiments. A superfluid fountain pump (6 in Fig. 1) was used to continuously fill the quartz beaker with HeII during the experiments. A liquid nitrogen-cooled quartz capillary (1 in Fig. 1) was used for the injection of impurity-helium (Im-He) gases into the beaker. The capillary extended from the top of the Dewar to 3 cm above the beaker, and the outlet of the

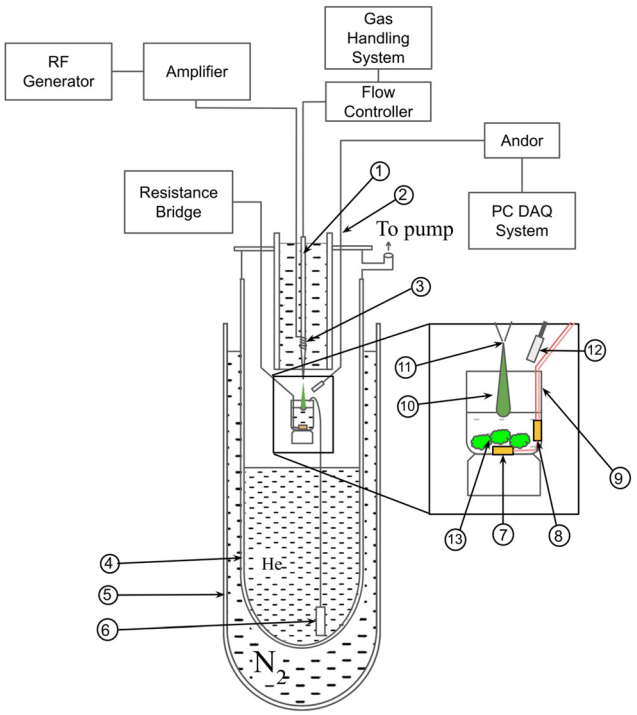

Fig. 1 Schematic of the experimental setup for the optical study of the luminescence of gas jets and collection of the neon nanoclusters: (1) quartz capillary, (2) optical fiber with spectral range of 200–1000 nm, (3) RF discharge resonator, (4) liquid helium Dewar, (5) liquid nitrogen Dewar, (6) fountain pump, (7) first thermometer, (8) second thermometer, (9) sample accumulation beaker, (10) N_2–Ne–He gas jet, (11) 0.75 mm orifice in the quartz capillary, (12) optical fiber input, (13) collection of neon nanoclusters.

quartz capillary was tapered and had a small orifice at the end, so that the exiting gases created a well-formed jet. Located just above the capillary orifice was a helical resonator (3 in Fig. 1), which facilitated radio frequency (RF) discharge of the gas mixtures used in this experiment. The resonator was operated at a frequency of ≈80 MHz and was supplied with 50 W of power.

An Oxford Instruments Andor optical spectrometer was used to register the emission spectra of the gas jet, as well as the accumulated samples. The Andor spectrometer measured wavelengths from 505 to 540 nm with a resolution of 0.03 nm. The Andor spectrometer measured the emission spectra from within the cryostat using a cryogenic bifurcating optical fiber (2 in Fig. 1) that extended into the cryostat, with the end directed toward the center of the beaker bottom.

The gas mixtures of N_2:Ne:He = 1:10:220, 1:20:400, 1:50:1000, 1:50:2500, and 1:1000:50 000 as well as Ne:He = 1:20, 1:50, 1:100, and 1:200 were used in these experiments. Gas mixtures were first prepared in a room-temperature gas handling system. These gas mixtures were then fed into the helium Dewar through the liquid nitrogen-cooled quartz capillary at a constant flow rate of $\approx 5 \times 10^{19}$ particles per s, maintained by a Brooks Model 5850E Mass Flow Controller. Each sample was then accumulated for a period of ≈20–25 min. During accumulation, the temperature of HeII in the beaker was 1.5 K. After the sample was accumulated, we stopped supplying the Im-He gas mixture and terminated the RF discharge. The spectra of nitrogen α-group luminescence decay were then registered. Two calibrated Lake Shore semiconductor thermometers were placed near the bottom of the beaker for the temperature measurements.

3 Experimental results

We studied the decay of the α-group spectra of N atoms stabilized in Ne nanoclusters. The luminescence decay was recorded at a temperature of ≈1.3 K. Fig. 2 and 3 show the integrated spectra of the α-group during the decay process. The N_2/Ne ratio in the impurity-helium gas mixtures was varied from 5% to 0.016%.

Fig. 2 shows spectra of samples prepared from the N_2–Ne–He gas mixtures, and Fig. 3 shows spectra for samples prepared from the Ne–He gas mixtures, where nitrogen was present only as an impurity in the He gas. In order to estimate the quantity of nitrogen impurity in He gas, we performed experiment in which we compared the integrated spectra of the sample produced from a nitrogen–neon–helium (N_2:Ne:He = 1:1000:50 000) and from a neon–helium (Ne:He = 1:50) gas mixtures. In the preparation of the first gas mixture, we used purified Ne gas using a liquid nitrogen trap and a known

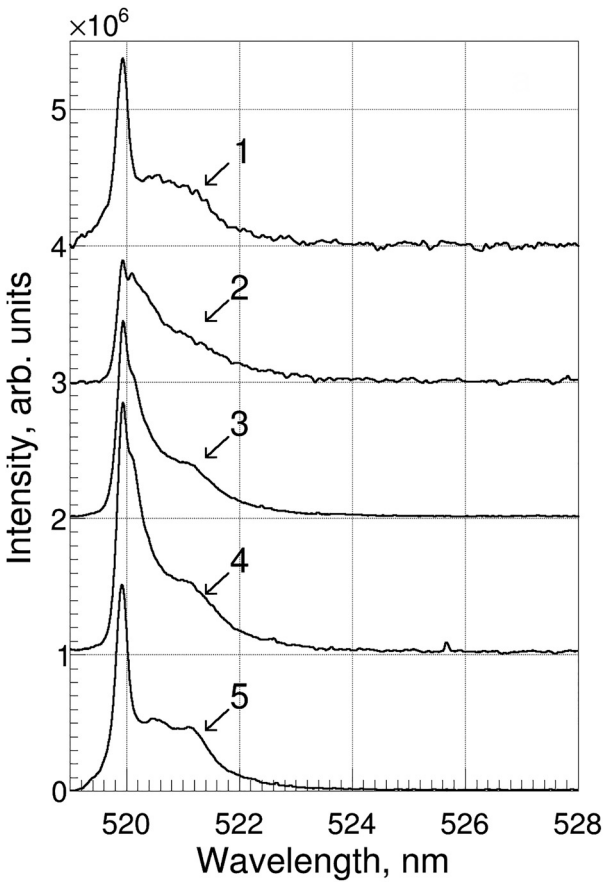

Fig. 2 Integrated spectra of nitrogen atom α-group luminescence decay for collections of neon nanoclusters doped with nitrogen atoms. Samples were formed by injecting the following gas mixtures into HeII: N_2:Ne:He = 1:10:220(1), 1:20:400(2), 1:50:1000(3), 1:50:2500(4), and 1:1000:50 000(5) (spectra were shifted along the *y*-axis for clarity).

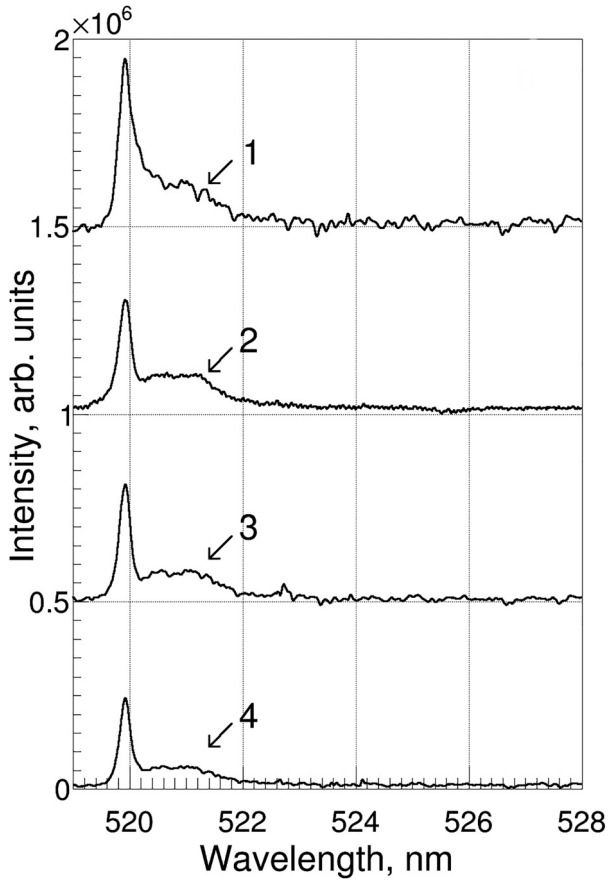

Fig. 3 Integrated spectra of nitrogen atom α-group luminescence decay for collections of neon nanoclusters. Samples were formed by injecting the following gas mixtures into HeII: Ne : He = 1 : 20(1), 1 : 50(2), 1 : 100(3), and 1 : 200(4). Nitrogen was present in the mixture as an impurity in the He gas. (Spectra were shifted along the *y*-axis for clarity).

quantity of added nitrogen gas. The ratio Ne/He, which determines the size of the Ne nanoclusters, was the same for both mixtures. The obtained integrated spectra for samples prepared from the above-mentioned two mixtures are shown in Fig. 4. Both spectra were obtained under similar experimental conditions and were almost identical after scaling the second spectra by a factor of 3.5. This experiment allowed us to determine the nitrogen content in the He gas, which we found to be equal to ≈8 ppm. All spectra presented in Fig. 2–4 have an approximately similar shape, with a greater intensity of the narrow line at $\lambda \approx 519.9$ nm. The intensities of the spectra decrease with the reduction of the nitrogen content in the gas mixture used for sample preparation.

Fig. 5 shows the dynamics of the α-group decay for the collection of nitrogen–neon nanoclusters prepared from three different gas mixtures. During the decay process, the shape of the α group spectra changed slightly, however the narrow line at $\lambda = 519.9$ nm was always the strongest in the spectra. The α-group spectra possessed a complex structure in the wavelength range 519–524 nm. The spectrum was fitted as the sum of seven components, shown in Fig. 6. Voigt functions were used to model each of the spectral components.

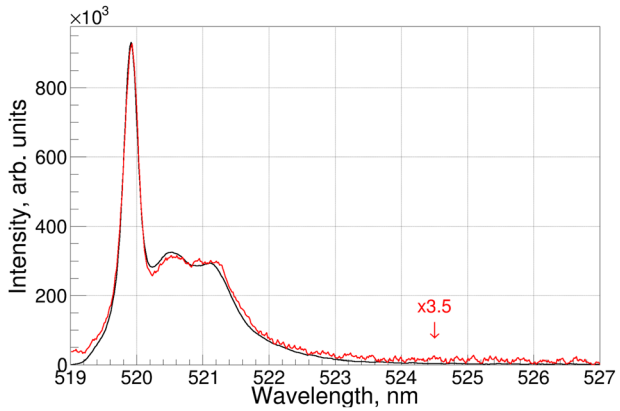

Fig. 4 Integrated spectra of α-group luminescence decay at $T \approx 1.3$ K for collection of nanoclusters formed by gas mixtures N_2 : Ne : He = 1 : 1000 : 50 000 (black line) and Ne : He = 1 : 50 (red line, scaled by the factor of 3.5).

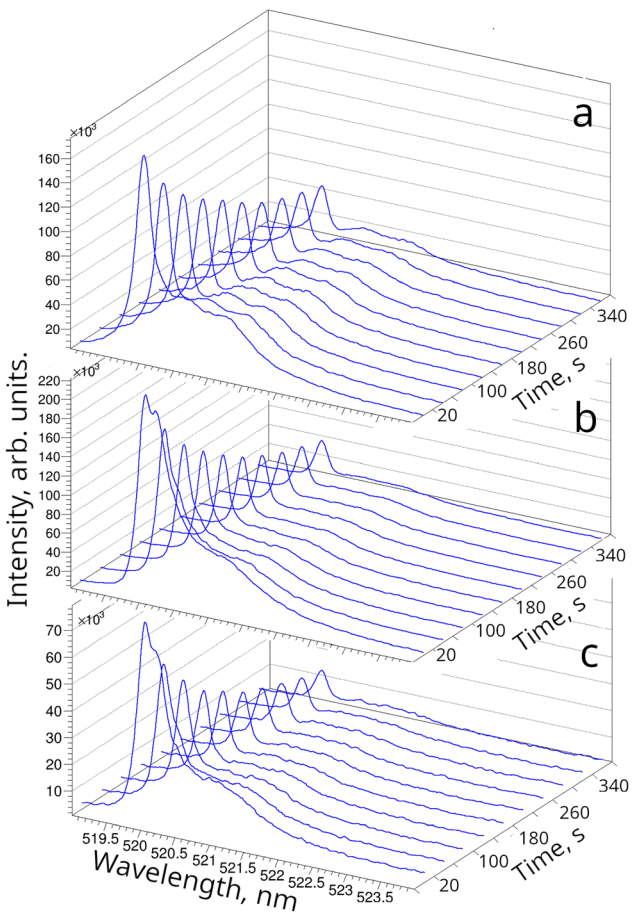

Fig. 5 Dynamics of the α-group intensity decay for the nitrogen–neon nanoclusters formed in HeII by condensation of different gas mixtures: (a) N_2 : Ne : He = 1 : 10 : 220, (b) N_2 : Ne : He = 1 : 50 : 1000, and (c) Ne : He = 1 : 20. Plots show the change in the shape and amplitude of the α-group after the discharge and gas mixture supply were turned off.

Fig. 6a shows the α-group spectrum at the beginning of the decay (during the first 10 seconds) and the corresponding seven fitting Voigt functions for the collection of nanoclusters

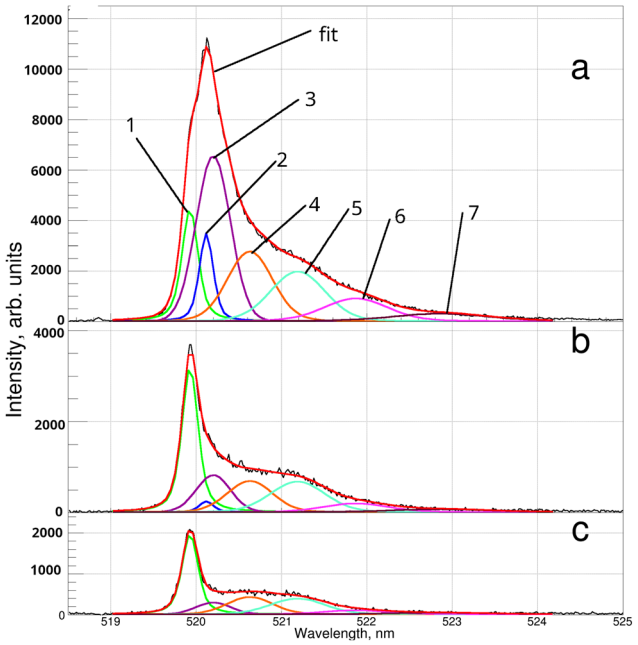

Fig. 6 Fit of the α-group luminescence spectra decay for collection of nanoclusters obtained by N_2 : Ne : He = 1 : 50 : 1000 gas mixture, at different moments after beginning of registration: (a) t = 10 s, (b) t = 120 s, and (c) t = 240 s. Spectra (black) were taken *via* an Andor spectrometer with a 1800 l mm^{-1} grating. The individual spectral components fitted by Voigt functions are shown by the following colors: 1 – green, 2 – blue, 3 – purple, 4 – orange, 5 – cyan, 6 – magenta, 7 – maroon. The sum of the seven components is shown as "fit" – red. The parameters for the spectra components obtained from the fits are shown in Table 1.

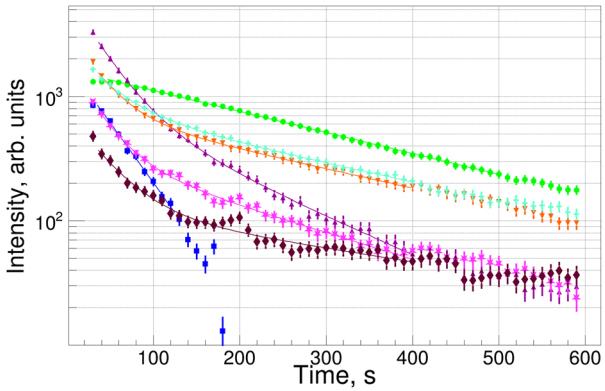

Fig. 7 Time dependence of α-group component amplitudes during decay process for collection of nanoclusters formed by N_2 : Ne : He = 1 : 50 : 1000 gas mixure: line at 519.92 nm – green circles, 520.14 nm – blue squares, 520.2 nm – purple up triangles, 520.63 nm – orange down triangles, 521.19 nm – cyan crosses, 521.87 nm – magenta stars, and 522.86 nm – maroon rhombuses. Decay times for each line are listed in Table 1.

prepared from the gas mixture N_2 : Ne : He = 1 : 50 : 1000. Fig. 6b shows the spectrum in the middle of the decay (120 s after beginning) and the seven corresponding fitting components. Fig. 6c shows the spectrum at the late stages of the decay (240 s after beginning) and seven fitting components.

In order to model the α-group spectra, we used the following approach. We first assumed that the positions and widths of each component of the spectra did not change during the decay process. Therefore, the function used for fitting the α group spectra during the early and later stages of the decay should only differ by the amplitudes of the components, not their shapes. In the first step of our analysis procedure, we fitted the early stage of the decay spectra with Voigt functions using seven components for which the position, width, and amplitude were left as free parameters. For the next steps, the decay spectra were split into 10 to 12 s intervals. Spectra recorded during each interval were fitted with a composite Voigt function, with the positions and widths of the components fixed to the values obtained in step one, while the amplitudes were left as free parameters.

For each of the individual components, amplitudes extracted from the fits have been fitted with a decay exponent or a sum of decay exponents, as shown in Fig. 7. Fig. 7 is presented in logarithmic scale on the y-axis, in which the exponents are straight lines. Only the blue line (fast decay) and green line (slow decay, narrow line) can be fitted by a straight line, and therefore can be represented by a single exponent. For other lines, we used the sum of two decaying exponents (fast $\tau \approx 30$ s and slow $\tau \approx 300$ s).

The same decay analysis procedure was used for all samples studied in this work. The results of these analyses are presented in Tables 1 and 2, where wavelengths, linewidths, and decay times for each of the components of the nitrogen α-group are listed.

Most of the spectral components presented in Tables 1 and 2 had a long decay time ranging from 224 to 332 s. Only the components at $\lambda \approx 520.1$ nm were found to have relatively short decay times ranging from 28 s to 58 s. The decay times for these components were attributed to the presence of N_2 molecules in the neon nanoclusters. For the samples with the largest content of nitrogen, the spectra of the α-group had stronger intensities, but during the decay process, the components that were influenced by nitrogen molecules decayed fastest. Fig. 8 shows the dynamics of the ratio of narrow line intensity to the total intensity of α-group spectra. For the samples with large content of nitrogen in neon nanoclusters (0.14–5%) the ratio at the beginning of decay was growing during ≈275 s and after reaching maximum was decreasing linearly. The initial growth of the ratio was due to the faster decay of α-group components, which were influenced by the presence of N_2 molecules in the neon nanoclusters.[45] The decay of components corresponding to N atoms surrounded by Ne atoms is much slower.[46] For samples with small (0.04–0.08%) content of nitrogen in neon nanoclusters, the weight of the narrow line linearly decreased in the decay process. This might be a consequence of longer decay times for the other components of α-group spectra for the latter samples.

The shapes of the α-group spectra in neon nanoclusters with strong maxima at $\lambda \approx 519.9$ nm were similar for all as-prepared samples studied in this work. Warming of the collection of neon nanoclusters from 1.3 K to 13 K initiated recombination of the stabilized nitrogen atoms and led to changes in the nanocluster structures. Fig. 9 shows the α-group spectra of nitrogen atoms in neon nanoclusters obtained during decay of

Table 1 Parameters of nitrogen atom α-group spectral components (centers, linewidths, decay times) extracted from the luminescence spectra fits of the nitrogen–neon nanoclusters. For each mixture, the sum of seven Voigt functions was used. The amplitudes obtained from fits at different stages of the sample luminescence decay were used to determine the characteristic decay times. For components 3–7, the exponents with two different characteristic times have been used

		N_2 : Ne : He gas mixtures (N_2/Ne ratio in the nanoclusters)				
Spectra components		1 : 10 : 220(10%)	1 : 20 : 400(5%)	1 : 50 : 1000(2%)	1 : 50 : 2500(2%)	1 : 1000 : 50 000(0.14%)
1	λ, nm	519.92(0.01)	519.92(0.01)	519.93(0.01)	519.91(0.02)	519.9(0.02)
	FWHM, nm	0.39(0.04)	0.22(0.05)	0.32(0.05)	0.28(0.03)	0.37(0.05)
	τ, s	**302(15)**	**271(12)**	**256(19)**	**279(9)**	**289(12)**
2	λ, nm	520.09(0.04)	520.1(0.05)	520.12(0.04)	520.1(0.05)	520.09(0.03)
	FWHM, nm	0.41(0.05)	0.26(0.03)	0.25(0.03)	0.23(0.03)	0.41(0.07)
	τ, s	**31(12)**	**47(11)**	**44(8)**	**58(8)**	**51(8)**
3	λ, nm	520.25(0.05)	520.2(0.05)	520.2(0.05)	520.2(0.04)	520.23(0.05)
	FWHM, nm	0.45(0.1)	0.47(0.7)	0.47(0.9)	0.47(0.11)	0.55(0.12)
	τ^*, s	50(12)	38(15)	34(14)	43(11)	31(15)
	τ, s	**283(25)**	**266(25)**	**180(65)**	**240(45)**	**290(35)**
4	λ, nm	520.55(0.07)	520.62(0.08)	520.63(0.07)	520.64(0.09)	520.59(0.12)
	FWHM, nm	0.65(0.12)	0.79(0.14)	0.65(0.13)	0.58(0.12)	0.6(0.12)
	τ^*, s	36(4)	32(6)	31(7)	43(10)	21(8)
	τ, s	**284(35)**	**246(68)**	**277(59)**	**290(75)**	**319(51)**
5	λ, nm	521.1(0.12)	521.22(0.13)	521.19(0.07)	521.16(0.13)	521.09(0.16)
	FWHM, nm	1.08(0.25)	0.83(0.24)	0.79(0.31)	1.06(0.37)	1.08(0.32)
	τ^*, s	55(12)	33(8)	40(12)	70(25)	74(26)
	τ, s	**273(56)**	**299(79)**	**280(75)**	**326(43)**	**329(37)**
6	λ, nm	521.94(0.17)	521.87(0.13)	521.87(0.15)	521.87(0.12)	521.91(0.16)
	FWHM, nm	1.26(0.4)	0.8(0.28)	0.97(0.34)	1.26(0.41)	1.26(0.34)
	τ^*, s	34(15)	35(17)	29(14)	49(20)	58(23)
	τ, s	**311(79)**	**224(109)**	**240(71)**	**331(45)**	**332(66)**
7	λ, nm	522.97(0.23)	522.78(0.14)	522.86(0.22)	522.9(0.19)	522.77(0.3)
	FWHM, nm	1.62(0.4)	1.62(0.4)	1.62(0.4)	1.62(0.4)	1.62(0.4)
	τ^*, s	22(12)	33(17)	38(15)	44(18)	25(13)
	τ, s	**300(112)**	**282(107)**	**294(121)**	**320(115)**	**320(97)**

the as-prepared sample made by N_2 : Ne : He = 1 : 50 : 2500 gas mixture and during destruction of this sample initiated by warming. As can be seen in Fig. 9, the spectrum of the α-group acquired during the destruction of the sample was completely different from that obtained for the as-prepared sample. The spectrum recorded during destruction had a maximum at $\lambda \approx 521.9$ nm. This spectrum corresponds to the α-group spectra of nitrogen atoms in N_2 nanoclusters.[11] The intensity of this spectrum was 20 times smaller than that of the as-prepared sample collected during the decay process. The spectrum obtained during sample destruction was the result of a series of processes. These processes include the recombination of nitrogen atoms with the formation of excited N_2 molecules and the successive transfer of their energy through nanoclusters to the nitrogen atoms surrounded by N_2 molecules.

4 Discussion

Recent experiments have provided evidence for the formation of solvation layers of solidified helium around neutral impurity atoms injected into superfluid helium (HeII).[38–44] Additionally, there have been theoretical predictions of the formation of solvation solid helium layers around impurities immersed into liquid helium[30,32,34,36,37] and even possibilities of the formation of quantum gels from single impurities surrounded by solvation layers of He atoms.[33,35]

The first attempts to create solidified helium were made by injecting gas discharge products into bulk HeII.[9–11] The high concentrations of stabilized nitrogen atoms inside superfluid helium obtained in these experiments were explained by the formation of metastable impurity-helium solids, in which the impurity atoms and molecules are surrounded by solid layers of helium due to van der Waals forces between the helium atoms and heavy impurities.[9–12] Subsequent X-ray and ultrasound investigations of these solid samples revealed only the presence of impurity nanoclusters, which form a porous structure inside HeII.[13–19] The high concentrations of nitrogen atoms in HeII were explained by the efficient stabilization of these atoms on the surfaces of N_2 nanoclusters.[5,21,22] Additionally, it was tentatively suggested that layers of solid helium are formed on the surfaces of the impurity nanoclusters. However, until now, there have been no direct experimental observations of the solid helium layers in the collection of nanoclusters immersed in HeII.

The goal of this work is to observe the influence of solid helium on the characteristics of nitrogen atoms stabilized on the surfaces of neon nanoclusters immersed into HeII. In our recent study on the luminescence of nitrogen–neon nanoclusters immersed in HeII, we observed a narrow line at λ = 519.9 nm in the N atom α-group spectra.[49] During the afterglow, this line became the dominant spectral component. It was tentatively suggested that this line can be assigned to N atoms on the surfaces of Ne nanoclusters surrounded by a solid layer of He atoms.

In order to provide additional evidence for this suggestion, we performed systematic studies of the luminescence of N atoms stabilized in neon nanoclusters with smaller nitrogen

Table 2 Parameters of nitrogen atom α-group spectral components (centers, linewidths, decay times) extracted from the luminescence spectra fits of the neon nanoclusters (same as described in Table 1). In neon–helium gas mixtures, molecular nitrogen is present as an impurity in helium gas at a level of 8 ppm. The absence of decay times for some components is due to their low intensity, resulting in the failed fits

		Ne : He gas mixtures (N_2/Ne ratio in the nanoclusters)			
Spectra components		1 : 20(0.016%)	1 : 50(0.04%)	1 : 100(0.08%)	1 : 200(0.16%)
1	λ, nm	519.91(0.02)	519.92(0.02)	519.91(0.03)	519.91(0.03)
	FWHM, nm	0.33(0.03)	0.38(0.04)	0.35(0.06)	0.34(0.05)
	τ, s	**254(25)**	**287(12)**	**293(17)**	**247(19)**
2	λ, nm	520.11(0.05)	520.09(0.06)	520.09(0.07)	520.09(0.08)
	FWHM, nm	0.26(0.05)	0.56(0.12)	0.61(0.15)	0.38(0.08)
	τ, s	**35(7)**	**38(7)**	**48(9)**	**28(5)**
3	λ, nm	520.27(0.05)	520.37(0.07)	520.4(0.12)	520.36(0.11)
	FWHM, nm	0.53(0.011)	0.71(0.013)	0.35(0.01)	0.58(0.016)
	τ*, s	37(8)	42(11)	19(12)	25(10)
	τ, s	**294(57)**	**280(63)**	**282(34)**	**279(45)**
4	λ, nm	520.65(0.12)	520.65(0.14)	520.64(0.12)	520.65(0.12)
	FWHM, nm	0.79(0.18)	0.68(0.21)	0.86(0.24)	0.62(0.23)
	τ*, s	30(9)	42(12)	52(34)	39(22)
	τ, s	**302(78)**	**320(87)**	**328(93)**	**263(120)**
5	λ, nm	521.16(0.17)	521.11(0.17)	521.17(0.22)	521.07(0.24)
	FWHM, nm	0.87(0.21)	1.08(0.25)	1.03(0.23)	1.03(0.35)
	τ*, s	65(24)	29(18)	72(42)	47(34)
	τ, s	**288(87)**	**305(71)**	**327(112)**	**312(120)**
6	λ, nm	521.88(0.2)	521.99(0.23)	522.01(0.22)	521.87(0.32)
	FWHM, nm	1.13(0.3)	1.23(0.31)	1.23(0.32)	1.25(0.34)
	τ*, s	31(15)	—	—	—
	τ, s	**312(125)**	—	—	—
7	λ, nm	523(0.5)	523(0.5)	523(0.5)	523(0.5)
	FWHM, nm	1.62(0.4)	1.6(0.4)	1.62(0.4)	1.62(0.4)
	τ*, s	31(11)	—	—	—
	τ, s	**300(125)**	—	—	—

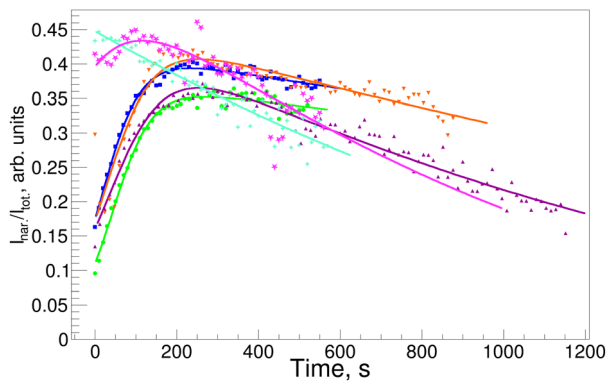

Fig. 8 Dynamics of the α-group narrow component (λ = 519.9 nm) weight. The weight is calculated as the ratio of the narrow component integral luminescence to the entire α-group luminescence. Presented data were obtained in experiments with different gas mixtures: N_2 : Ne : He = 1 : 20 : 400 – green circles, N_2 : Ne : He = 1 : 50 : 1000 – blue squares, N_2 : Ne : He = 1 : 50 : 2500 – purple up triangles, N_2 : Ne : He = 1 : 1000 : 50 000 – orange down triangles, Ne : He = 1 : 50 – teal crosses, and Ne : He = 1 : 100 – magenta stars.

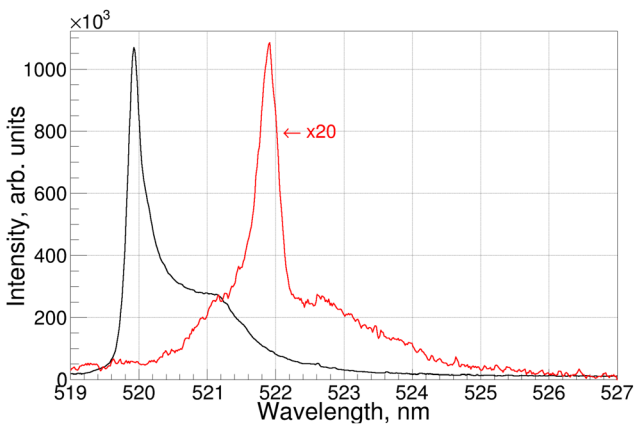

Fig. 9 Integrated spectra of α-group luminescence decay at $T \approx 1.3$ K for the collection of nanoclusters formed by gas mixture N_2 : Ne : He = 1 : 50 : 2500 (black line) and integrated spectra of α-group during explosive destruction of this collection of nanoclusters initiated by warming from 1.3 K to $T \approx 13$ K (red line).

contents than those used in the previous work. In this work, N_2/Ne ratio in nanoclusters was varied in the range from 5% to 0.016%. For all spectra obtained in this work, the intensity of the narrow line at λ = 519.9 nm was maximal. Furthermore, the relative intensity of this line increased relative to all other components of the α-group as the content of nitrogen in Ne nanoclusters was reduced (see Fig. 2 and 3). According to ESR studies of atoms in the nanoclusters, the majority of the N atoms were stabilized on the surfaces of nanoclusters.[20–22] Therefore, the strongest line in the α-group at λ = 519.9 nm might be assigned to the N atoms trapped on the surfaces of Ne nanoclusters. The enhancement of the narrow line and the increase in relative intensity upon reducing the nitrogen content in nanoclusters support the assignment of the narrow line to N atoms on the surfaces of neon nanoclusters. With lower N atom content, a larger fraction of atoms was stabilized on the surfaces of the Ne nanoclusters.

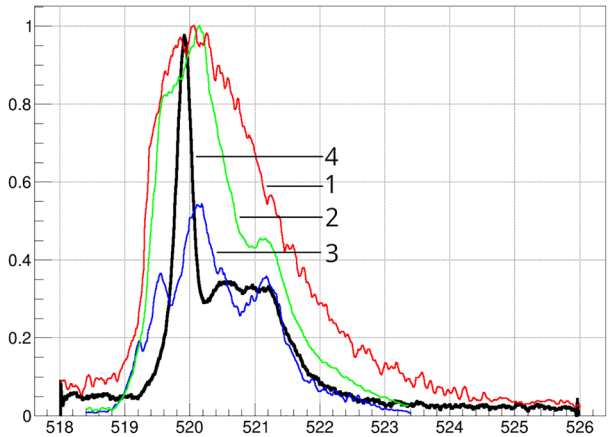

Fig. 10 Comparison of the structure of the α-group in N_2/Ne films containing 1% (1 – red curve[48]) and 0.05% (2 – green curve and 3 – blue curve[47]) of nitrogen with the α-group of neon nanoclusters containing 0.04% of nitrogen during afterglow (4 – black curve). Spectra 1 and 2 were obtained in the process of bombarding N_2/Ne films by low-energy electrons. Spectrum 3 was taken during afterglow, 210 s after registration of spectrum 2.

When neon nanoclusters are immersed into HeII, the solid helium layers are formed on the surfaces of nanoclusters according to experimental[5,53] and theoretical studies.[32] The van der Waals interaction between Ne atoms on the surfaces of the nanoclusters and surrounding helium atoms is strong enough to form solid helium layers surrounding neon nanoclusters. These first helium layers are definitely solid because the resulting pressure in these helium layers substantially exceeds the pressure needed to solidify liquid helium.[32,53,54] We can expect that only in the second or third layers, for which the attraction of He atoms to Ne nanoclusters is weaker, it is possible to observe fluxional[55] or supersolid behavior.[56] Therefore, neon nanoclusters immersed into HeII are surrounded by a ≈1–2 layers of solid helium.[5,53] It is natural to expect that characteristics of N atoms stabilized on the surfaces of Ne nanoclusters should be influenced by the close proximity of solid helium layers, and the shape of the α-group luminescence of nitrogen–neon nanoclusters immersed in HeII should be different from that of solid N_2/Ne films.

We can compare spectra of the α-group luminescence of nitrogen–neon nanoclusters immersed in HeII, and the luminescence of N atoms in solid N_2/Ne films (see Fig. 10).[47,48] The α-group spectra of N atoms stabilized in mixed N_2/Ne films were studied at a temperature of 7.8 K upon low energy (less than 500 eV) electron excitation for different concentrations of N_2 molecules ranging from 100% to 0.05%.[47,48] Substantial transformations of the α group spectra were observed when the concentration of the N_2 molecules was changed from 100% to 1%. At N_2 concentrations equal to 7%, the α group spectrum had two maxima at λ = 521 nm and λ = 523 nm, but at 1% N_2 concentration, the spectra become very broad with only one maximum at λ = 520 nm (see 1 in Fig. 10).[48] Further reduction of the concentration of N_2 in the neon film to 0.05%, resulted in the observation of three maxima during excitation by electrons (see 2 in Fig. 10) and five maxima in the following afterglow (see 3 in Fig. 10), when the electron flux was terminated.[47] In the latter spectrum, two blue-shifted maxima were observed at wavelengths λ = 519.26 nm and λ = 519.59 nm, with decay times less than 340 s. The rest of the lines in this spectrum were at λ = 520.11 nm, 520.46 nm, 521.07 nm, and their decay times were equal to 340 s.[47] The α-group spectra of neon nanoclusters (see 4 in Fig. 10) was substantially different from the α-group spectra of N_2/Ne solid films with similar nitrogen content.

The α-group spectra of N atoms in nitrogen–neon nanoclusters immersed in HeII were previously studied during the process of accumulation[57] and during the decay process.[49] In experiments, when the α-group was studied during the accumulation process, the content of N_2 molecules in neon nanoclusters was varied from 30% to 3%. All spectra obtained in these experiments had only one maximum, but the position of this maximum shifted from λ = 521 nm to λ = 520 nm, when the concentration of N_2 molecules was reduced from 30% to 3%.[57]

In the present work, the ratio N_2/Ne in neon nanoclusters was varied from 5% to 0.016%, and it was found that all α-group spectra had a maximum at λ = 519.9 nm. The dynamics of the intensity ratio of the narrow component and the entire α-group spectra shown in Fig. 7 provide information about nitrogen molecules captured in the neon nanoclusters. In the nanoclusters with the ratio N_2/Ne in the range 5–0.14%, the N atoms can be trapped in the vicinity of N_2 molecules inside neon nanoclusters. For these atoms the decay times are rather small ($\tau \leq 30$ s).[45] As a result, the intensity ratio of the narrow component to the entire α-group spectra grew during the first 275 s of afterglow as seen in Fig. 7. When all N atoms in nanoclusters influenced by N_2 molecules had decayed, only the emission of the N atoms surrounded by Ne atoms and the N atoms on the surfaces of Ne nanoclusters provided the afterglow characterized by long decay times ($\tau \approx 300$ s). During this period of afterglow, the weight of the narrow line decreased linearly, demonstrating a longer decay time of N atoms surrounded by Ne atoms in the interior of the nanoclusters, in comparison with that of N atoms on the surfaces of Ne nanoclusters. For nanoclusters with a smaller N_2/Ne ratio equal to 0.08% (gas mixture Ne : He = 1 : 100), only a small influence of N_2 molecules was observed during a shorter period of 100 s. Finally, at the N_2/Ne ratio equal to 0.04% (gas mixture Ne : He = 1 : 50), there was no influence of N_2 molecules on the afterglow of Ne nanoclusters. From the beginning of the afterglow, the weight of the narrow line was linearly decreased. Therefore, we can conclude that all N_2 molecules were dissociated in the discharge and only single N atoms were captured in the interior and on the surface of Ne nanoclusters formed by condensation of the Ne : He = 1 : 50 gas mixture.

The position of the narrow line is close to the emission of N atoms in the gas phase (λ = 519.8 and λ = 520 nm[58]). It is known that the shift of the α-group in solid rare gas matrices relative to the undisturbed position of the lines in the gas phase is linearly proportional to the polarizability of the atoms forming solid matrices.[57] The polarizability of He atoms is almost twice smaller than that of Ne atoms. Therefore, we might expect that the position of the α-group in a solid helium matrix should be closer to the undisturbed position of the lines in the gas phase.

This is exactly what we observed in our experiments: the position of the most intense narrow line in the α-group spectra was very close to the undisturbed position of the lines in the gas phase. Even though the position of the narrow line was close to the position of the undisturbed atoms, the lifetime for this line was substantially less than that for undisturbed atoms, showing the influence of the environment. This provides evidence that this line corresponds to the emissions of the $N(^2D)$ atoms for which the influence of the surrounding environment is less than for $N(^2D)$ atoms in a Ne matrix. This might be considered as further evidence of the N atoms being surrounded by a solid helium layer.

The third evidence of the presence of solid helium layers in the vicinity of emitting $N(^2D)$ atoms originated from the stability studies of nitrogen–neon nanoclusters with small nitrogen content. The solid helium layers were stable when the collections of Ne nanoclusters were immersed in HeII at $T \approx 1.5$ K. Removing the nanoclusters from HeII by evaporating all HeII from the beaker and warming above 4.2 K initiates the diffusion of atoms within the nanoclusters and the recombination of stabilized nitrogen atoms. The energy released from N atom recombination accelerates the structural changes in neon nanoclusters and the destruction of solid helium layers, which should alter the emission spectra of N atoms. Indeed, the spectra of the α group observed during the destruction of neon nanoclusters are completely different from those observed during the luminescence decay at $T \approx 1.3$ K (see Fig. 9). The spectra of the α group during the destruction of Ne nanoclusters were found to be identical to those observed in $N–N_2$ nanoclusters,[11] providing evidence for the major role of N_2 molecules in the emitting $N(^2D)$ atoms during the nanocluster destruction process.

5 Conclusions and future work

We studied the α-group spectra of nitrogen atoms stabilized in neon nanoclusters immersed in bulk HeII. The spectra were in the wavelength range 519–523 nm, and their line-shapes were asymmetric with an enhanced narrow peak at $\lambda = 519.9$ nm and an unresolved band with smaller intensity. We modeled the spectra as a superposition of seven components represented by Voigt functions. The position of the most intense narrow line, at $\lambda = 519.9$ nm, was remarkably close to the position of the emission line of nitrogen atoms in the gas phase at $\lambda = 519.8$ nm.[58] This intense narrow line observed α-group spectra might be assigned to the most populated trapping sites of N atoms in the neon nanoclusters. Earlier ESR studies found that the majority of nitrogen atoms were trapped on the surfaces of neon nanoclusters.[20–22] Therefore, it is natural to assign this narrow line to the nitrogen atoms trapped on the surfaces of neon nanoclusters immersed into HeII. It is also known that neon nanoclusters immersed in HeII were covered by at least one layer of solid helium.[32,54] All experimental findings mentioned above allow the assignment of the narrow line of the α-group spectra to nitrogen atoms trapped on the surfaces of neon nanoclusters, surrounded by a layer of solid helium.

The shifts of the positions of the α-group lines in solid rare gas matrices relative to the position of the undisturbed gas phase lines, for nitrogen atoms, were proportional to the polarizability of the atoms forming solid matrices.[57] For the case of trapping N atoms in a solid helium matrix, the position of the α-group should be closest to the gas phase position for nitrogen atoms. This tendency indirectly supports our assignment of the narrow line to the trapping sites influenced by a solid helium layer.

During warming, the spectra of the α-group changed drastically. The narrow line at $\lambda = 519.9$ nm, present in spectra of as-prepared samples, disappeared, and a broad spectrum with a maximum at $\lambda = 521.9$ nm was observed. The transformation of the α-group spectra can be explained by changing the environment of the emitting nitrogen atoms. During the warming-up process, the unique fragile environment containing the solid helium layer was destroyed, and a stable and stronger interacting surrounding containing N_2 molecules was formed.

The three experimental evidences, which include the close to gas-phase line position and narrow linewidth of the α-group component at $\lambda = 519.9$ nm, the exponential decay of this component with a characteristic time of 280 s as well as disappearance of this component upon warming up from 1.3 K to 13 K, allow us to conclude that the α-group component at $\lambda = 519.9$ nm corresponds to the nitrogen atoms stabilized on the surfaces of neon nanoclusters and surrounded by layers of solid helium. The evidence for solid helium layers on the neon nanoclusters obtained in this work was supported by previous theoretical[30–37] and experimental studies.[38–44]

In future experiments, we plan direct registration of solid helium formed on the surfaces of impurity nanoclusters. For this purpose, we will study collections of neon nanoclusters with smaller sizes. It is known that dilution of impurities by helium gas in condensed impurity-helium mixtures allows the formation in HeII the collections of nanoclusters with smaller sizes.[13,14] In the past, the gas mixtures with more than 1% of impurities had been used. As a result, the average size of nanoclusters was of order 5 nm ($\approx$2000 impurity atoms/molecules).[13,14] We plan the preparation of neon nanoclusters by using impurity helium gas mixtures with Ne/He ratios from 0.1% to 0.01%. The ratio of the quantity of He atoms in solid helium layers to the quantity of Ne atoms in the samples will be larger in the collection of nanoclusters with the smaller sizes. The method of X-ray diffraction can be used for the determination of the neon nanocluster sizes and for the direct observation of the solid helium on the surface of neon nanoclusters. Earlier experiments showed that the collection of neon nanoclusters can survive after being removed from liquid helium, forming dry samples.[13] For dry samples, the background signal from liquid helium will be considerably reduced, providing a better chance for detection of the X-ray diffraction signal from the solid helium layers.

Author contributions

Oleksandr Korostyshevskyi: investigation, formal analysis, software, writing – original draft, writing – review & editing. Cameron

Wetzel: investigation, writing – review & editing. David M. Lee: supervision, writing – review & editing, funding acquisition. Vladimir V. Khmelenko: project administration, conceptualization, investigation, writing – original draft, writing – review & editing, funding acquisition.

Conflicts of interest

There are no conflicts to declare.

Data availability

Data and code for this article, including raw data for Andor spectrometer, as well as temperature and pressure logs, are available at https://osf.io/4qjp3/overview.

Acknowledgements

This material is based upon work supported by the National Science Foundation under grant DMR-2104756.

References

1 B. Tabbert, H. Günther and G. zu Putlitz, *J. Low Temp. Phys.*, 1997, **109**, 653–707.
2 J. P. Toennies and A. F. Vilesov, *Annu. Rev. Phys. Chem.*, 1998, **49**, 1–41.
3 S. I. Kanorsky and A. Weis, *Adv. At., Mol., Opt. Phys.*, 1998, **38**, 87–120.
4 J. P. Toennies and A. F. Vilesov, *Angew. Chem., Int. Ed.*, 2004, **43**, 2622–2648.
5 V. V. Khmelenko, H. Kunttu and D. M. Lee, *J. Low Temp. Phys.*, 2007, **148**, 1–31.
6 P. Moroshkin, A. Hofer and A. Weis, *Phys. Rep.*, 2008, **469**, 1–57.
7 J. Jortner, L. Meyer, S. A. Rice and E. G. Wilson, *Phys. Rev. Lett.*, 1964, **12**, 415–416.
8 E. B. Gordon, L. P. Mezhov-Deglin and O. F. Pugachev, *J. Exp. Theor. Phys. Lett.*, 1974, **19**, 63–65.
9 E. B. Gordon, L. P. Mezhov-Deglin, O. F. Pugachev and V. V. Khmelenko, *Cryogenics*, 1976, **16**, 555–557.
10 E. B. Gordon, V. V. Khmelenko, A. E. Popov, A. A. Pelmenev and O. F. Pugachev, *Chem. Phys. Lett.*, 1989, **155**, 301–304.
11 R. Boltnev, E. Gordon, V. Khmelenko, I. Krushinskaya, M. Martynenko, A. Pelmenev, E. Popov and A. Shestakov, *Chem. Phys.*, 1994, **189**, 367–382.
12 E. B. Gordon and A. F. Shestakov, *Low Temp. Phys.*, 2000, **26**, 1–23.
13 V. Kiryukhin, B. Keimer, R. E. Boltnev, V. V. Khmelenko and E. B. Gordon, *Phys. Rev. Lett.*, 1997, **79**, 1774–1777.
14 V. Kiryukhin, E. P. Bernard, V. V. Khmelenko, R. E. Boltnev, N. V. Krainyukova and D. M. Lee, *Phys. Rev. Lett.*, 2007, **98**, 195506.
15 N. V. Krainyukova, R. E. Boltnev, E. P. Bernard, V. V. Khmelenko, D. M. Lee and V. Kiryukhin, *Phys. Rev. Lett.*, 2012, **109**, 245505.
16 S. I. Kiselev, V. V. Khmelenko, D. A. Geller, D. M. Lee and J. R. Beamish, *J. Low Temp. Phys.*, 2000, **119**, 357–366.
17 S. Kiselev, V. Khmelenko, D. Geller, J. Beamish and D. Lee, *Phys. B*, 2000, **284–288**, 105–106.
18 S. I. Kiselev, V. V. Khmelenko and D. M. Lee, *J. Low Temp. Phys.*, 2000, **121**, 671–676.
19 S. I. Kiselev, V. V. Khmelenko and D. M. Lee, *Low Temp. Phys.*, 2000, **26**, 641–648.
20 S. Mao, R. E. Boltnev, V. V. Khmelenko and D. M. Lee, *Low Temp. Phys.*, 2012, **38**, 1037–1042.
21 C. K. Wetzel, D. M. Lee and V. V. Khmelenko, *J. Low Temp. Phys.*, 2024, **215**, 294–311.
22 C. K. Wetzel, D. M. Lee and V. V. Khmelenko, *J. Low Temp. Phys.*, 2025, **220**, 25–50.
23 A. Scheidemann, J. P. Toennies and J. A. Northby, *Phys. Rev. Lett.*, 1990, **64**, 1899–1902.
24 T. E. Gough, M. Mengel, P. A. Rowntree and G. Scoles, *J. Chem. Phys.*, 1985, **83**, 4958–4961.
25 S. Goyal, D. L. Schutt and G. Scoles, *Phys. Rev. Lett.*, 1992, **69**, 933–936.
26 R. Fröchtenicht, J. Toennies and A. Vilesov, *Chem. Phys. Lett.*, 1994, **229**, 1–7.
27 M. Hartmann, R. E. Miller, J. P. Toennies and A. Vilesov, *Phys. Rev. Lett.*, 1995, **75**, 1566–1569.
28 C. Callegari and W. E. Ernst, *Helium Droplets as Nanocryostats for Molecular Spectroscopy—from the Vacuum Ultraviolet to the Microwave Regime*, John Wiley & Sons, Ltd, 2011.
29 A. Slenczka and J. P. Toennies, *Molecules in Superfluid Helium Nanodroplets*, Springer, Cham, 2022.
30 K. E. Kürten and J. W. Clark, *Phys. Rev. B: Condens. Matter Mater. Phys.*, 1985, **32**, 2952–2959.
31 Y. Kwon, P. Huang, M. V. Patel, D. Blume and K. B. Whaley, *J. Chem. Phys.*, 2000, **113**, 6469–6501.
32 F. Dalfovo, *Z. Phys. D: At., Mol. Clusters*, 1994, **29**, 61–66.
33 J. Eloranta, *Phys. Rev. B: Condens. Matter Mater. Phys.*, 2008, **77**, 134301.
34 J. Eloranta, *Low Temp. Phys.*, 2011, **37**, 384–386.
35 J. Eloranta, *J. Low Temp. Phys.*, 2011, **162**, 718–723.
36 M. Blancafort-Jorquera, A. VilÃ and M. GonzÃ¡lez, *Phys. Chem. Chem. Phys.*, 2019, **21**, 24218–24231.
37 F. Coppens, F. Ancilotto, M. Barranco, N. Halberstadt and M. Pi, *Phys. Chem. Chem. Phys.*, 2019, **21**, 17423–17432.
38 A. Przystawik, S. Göde, T. Döppner, J. Tiggesbäumker and K.-H. Meiwes-Broer, *Phys. Rev. A: At., Mol., Opt. Phys.*, 2008, **78**, 021202.
39 S. Göde, R. Irsig, J. Tiggesbäumker and K.-H. Meiwes-Broer, *New J. Phys.*, 2013, **15**, 015026.
40 L. Kazak, S. Göde, K.-H. Meiwes-Broer and J. Tiggesbäumker, *J. Phys. Chem. A*, 2019, **123**, 5951–5956.
41 L. Kazak, K.-H. Meiwes-Broer and J. Tiggesbäumker, *Phys. Chem. Chem. Phys.*, 2022, **24**, 23350–23356.
42 R. M. P. Tanyag, D. Verma and A. F. Vilesov, *J. Chem. Phys.*, 2025, **162**, 091101.

43 M. Trejo, A. Clifford, E. G. Alfonso, N. Halberstadt, L. Xue and W. Kong, *J. Chem. Phys.*, 2024, **161**, 054306.
44 A. Clifford, M. Trejo, J. Zhang, X. Li, L. Xue and W. Kong, *J. Chem. Phys.*, 2025, **163**, 084310.
45 O. Oehler, D. A. Smith and K. Dressler, *J. Chem. Phys.*, 1977, **66**, 2097–2107.
46 D. S. Tinti and G. W. Robinson, *J. Chem. Phys.*, 1968, **49**, 3229–3245.
47 R. J. Sayer, R. H. Prince and W. W. Duley, *Phys. Status Solidi B*, 1981, **105**, 727–738.
48 R. J. Sayer, R. H. Prince and W. W. Duley, *Phys. Status Solidi B*, 1981, **106**, 249–258.
49 O. Korostyshevskyi, C. Wetzel, I. V. Borzenets, D. M. Lee and V. V. Khmelenko, *J. Low Temp. Phys.*, 2025, **220**, 158–168.
50 R. E. Boltnev, I. B. Bykhalo, I. N. Krushinskaya, A. A. Pelmenev, V. V. Khmelenko, S. Mao, A. Meraki, S. C. Wilde, P. T. McColgan and D. M. Lee, *J. Phys. Chem. A*, 2015, **119**, 2438–2448.
51 A. Meraki, S. Mao, P. T. McColgan, R. E. Boltnev, D. M. Lee and V. V. Khmelenko, *J. Low Temp. Phys.*, 2016, **185**, 269–286.
52 O. Korostyshevskyi, C. K. Wetzel, D. M. Lee and V. V. Khmelenko, *Low Temp. Phys.*, 2024, **50**, 722–732.
53 E. Cheng, M. W. Cole, W. F. Saam and J. Treiner, *Phys. Rev. B: Condens. Matter Mater. Phys.*, 1992, **46**, 13967–13982.
54 J. S. Dugdale and J. P. Franck, *Philos. Trans. R. Soc., A*, 1964, **257**, 1–29.
55 J. A. Davies, C. Schran, F. Brieuc, D. Marx and A. M. Ellis, *Phys. Rev. Lett.*, 2023, **130**, 083001.
56 J. C. A. Matos, P. Giannakeas, M. Ciardi, T. Pohl and J. M. Rost, *Phys. Rev. Lett.*, 2025, **134**, 186001.
57 R. E. Boltnev, E. B. Gordon, V. V. Khmelenko, M. V. Martynenko, A. A. Pelmenev, E. A. Popov and A. F. Shestakov, *J. Chem. Phys.*, 1995, **92**, 362–383.
58 B. D. Sharpee, T. G. Slanger, P. C. Cosby and D. L. Huestis, *Geophys. Res. Lett.*, 2005, **32**, L12106.

